# Surface Morphology during Multilayer Epitaxial Growth of Ge(001)

Joseph E. Van Nostrand, S. Jay Chey, M.-A. Hasan, David G. Cahill, and J. E. Greene
*Department of Materials Science, The Materials Research Laboratory, University of Illinois, Urbana, Illinois 61801*
(Received 11 July 1994; revised manuscript received 6 October 1994)

The surface morphology of Ge(001) films grown by molecular beam epitaxy on a Ge(001) substrate is measured using scanning tunneling microscopy. Growth mounds are observed for single crystal films deposited at temperatures of 60–230 °C and film thicknesses of 5 nm to 1 $\mu$m. With increasing growth temperature, the average separation between mounds becomes increasingly well defined, increasing from less than 10 nm at 60 °C to nearly 200 nm at 230 °C. This regular arrangement of growth mounds is inconsistent with the self-affine growth morphology predicted by most kinetic roughening models.

PACS numbers: 61.50.Cj, 68.55.Bd, 68.55.Jk

Novel thin film structures synthesized by molecular beam epitaxy (MBE) have found a wide variety of applications in science and technology. Smooth and abrupt interfaces between epitaxial layers are often a critical factor in determining device performance but the fabrication of such interfaces places conflicting demands on the growth conditions. Reducing the growth temperature reduces atom diffusion rates responsible for the intermixing of layers and dopant segregation and therefore facilitates the synthesis of abrupt transitions between layers [1]. Unfortunately, a low growth temperature also leads to multilayer growth [2] with an inherent increase in interface roughness.

The roughening of surfaces during epitaxial growth has been the subject of extensive theoretical study [3]. One approach to this problem is the dynamic scaling hypothesis, often termed kinetic roughening, where the growth surface is assumed to evolve into a temporal and scale invariant structure. Kinetic roughening is observed in Monte Carlo simulations of growth and in the solutions of partial differential equations that are thought to describe the essential physics of the microscopic growth processes [3,4]. Many experiments on surface roughness during thin film growth have been interpreted in the context of the dynamic scaling hypothesis. Scaling exponents are extracted from microscopy or diffraction measurements of the surface morphology [5–13].

We observe that the surface topography of Ge(001) grown by MBE on Ge(001) substrates is dominated by growth mounds that are separated from each other by a remarkably well defined, single length scale. This formation of a regular pattern of growth mounds is inconsistent with the self-affine morphology predicted by the dynamic scaling hypothesis.

Regular patterns of growth mounds have, however, been generated in recent computer simulations and theory [14] that stress the importance of a diffusion bias [4] on the evolution of surface roughness during epitaxial growth by molecular beams. The term diffusion bias, introduced by Villain [4], refers to the fact that the adatom diffusion current on a vicinal surface is not zero if an asymmetry exists in the kinetics of adatom attachment to steps. Field-ion microscopy of W and Ir surfaces clearly shows that adatom attachment to a descending step occurs at a smaller rate than adatom attachment at an ascending step [15,16]. The presence of a diffusion bias is predicted to produce instabilities in the propagation of straight steps [17] and in the growth morphology of singular surfaces [4,14].

Anisotropic growth mounds were recently observed experimentally during MBE growth of GaAs(001) [14,18, 19], and a similar surface morphology develops during growth of InP(001) using metalorganic MBE [10,20]. Our results for Ge(001) demonstrate that the formation of growth mounds is also prevalent during growth on the (001) surface of a diamond structure crystal and extends previous work to a wide range of growth temperature and in-plane length scale of the surface roughness.

Ge(001) wafers from Eagle-Picher Research Laboratory are cleaned using repeated ozone-assisted oxidation and removal of the oxide in water [21]. Samples are typically $1.5 \times 1.5$ cm and are In bonded to a 3 in. diameter Mo sample block. The final oxide layer is removed in the MBE growth chamber, base pressure $\simeq 10^{-10}$ Torr, by degassing the sample and sample holder for 90 min at 200 °C followed by oxide desorption for 30 min at 450 °C [21].

Prior to the low temperature growth experiments, a 100 nm thick buffer layer is deposited at 365 °C; a growth rate of 0.1 nm sec$^{-1}$ is used for all depositions. Growth temperatures above 150 °C are determined using an infrared pyrometer which is calibrated using a thermocouple bonded to a Ge test sample. To determine the growth temperature at $T < 150$ °C, we calibrate a thermocouple that is pressed against the Mo sample block versus a thermocouple bonded to a test Ge sample. During deposition, the chamber pressure rises to $\simeq 2 \times 10^{-9}$ Torr. The dominant components of the background gas are typically $1.4 \times 10^{-9}$ Torr of $H_2$, $2.5 \times 10^{-10}$ Torr of $H_2O$, and $1.4 \times 10^{-10}$ Torr of CO + $N_2$ measured using a mass spectrometer in line of site with the Ge electron beam evaporation source. We have not experimentally determined the effects of these levels of residual gas contamination on the growth morphology of Ge, but we note that a recent study of the influence of hydrogen on MBE growth of Si(001) shows that nearly a full monolayer of adsorbed hydrogen is required to alter the growth behavior [22].

0031-9007/95/74(7)/1127(4)$06.00 © 1995 The American Physical Society 

After growth, samples are moved to the scanning tunneling microscope analysis chamber, base pressure $\simeq 10^{-10}$ Torr, through a separately pumped UHV transfer line. The data reported below were acquired at negative sample bias between 1.5 and 2.5 V. We use chemically etched PtIr probe tips with a nominal tip radius of <50 nm.

The structure of the Ge(001) surface after oxide desorption [21] and after growth of the buffer layer is shown in Fig. 1. Buffer layer growth at 365 °C smooths the roughness of the substrate produced by oxide desorption and creates a nearly ideal surface with large terraces separated by atomic height steps. The average terrace width, 130 nm, reflects the miscut of the Ge crystal, 0.07° in the ⟨110⟩ direction. Smaller area scans of the buffer layer reveal the expected $2 \times 1$ dimer reconstruction with a low defect density, <1%.

Images of growth morphologies during multilayer growth are displayed in Fig. 2. The observation of growth mounds over a range of growth temperatures, 60–230 °C, requires the use of a wide range of film thicknesses. The critical thickness for epitaxial growth [23–25] sets an upper limit to the film thickness we can use in our experiments; for example, the maximum thickness for a defect-free epitaxial layer of Ge(001) at 60° is ~5 nm [25]. Also, as we increase the growth temperature we need increasingly thick films to observe well-defined growth mounds. For example, at 155° a 5 nm thick film shows multilayer growth but the peak-to-peak surface roughness is only 3 monolayers. A much thicker film, data for a 100 nm thick film are shown as Fig. 2(c), is required for the growth mounds to clearly develop.

The surfaces shown in Fig. 2 were also characterized by reflection-high-energy-electron-diffraction (RHEED); a $2 \times 1$ pattern was visible in each of the diffraction patterns. Large surface roughness often precludes scanning tunneling microscopy (STM) observation of surface reconstructions, but we were able to image dimer rows at the surfaces of the films shown in Figs. 2(a) and 2(d). These data, in combination with previous cross-sectional transmission electron microscopy (XTEM) studies of low temperature epitaxy of Ge(001) [25], allow us to conclude that the surface morphologies shown in Fig. 2 are for single crystal Ge with a predominately (001) orientation.

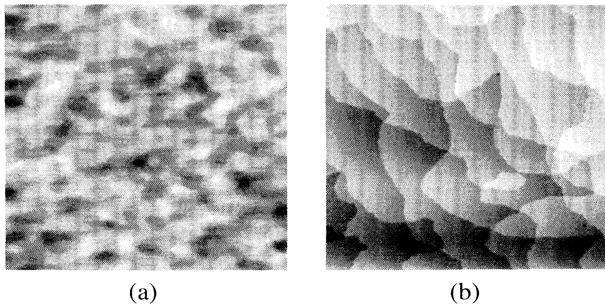


FIG. 1. STM images of Ge(001) following (a) oxide desorption and annealing at 450 °C and (b) growth of a 100 nm thick buffer layer at 365 °C. The $x$-$y$ range of both images is 1 $\mu$m and the $x$ and $y$ axes of the images are aligned with the ⟨100⟩ crystal directions.

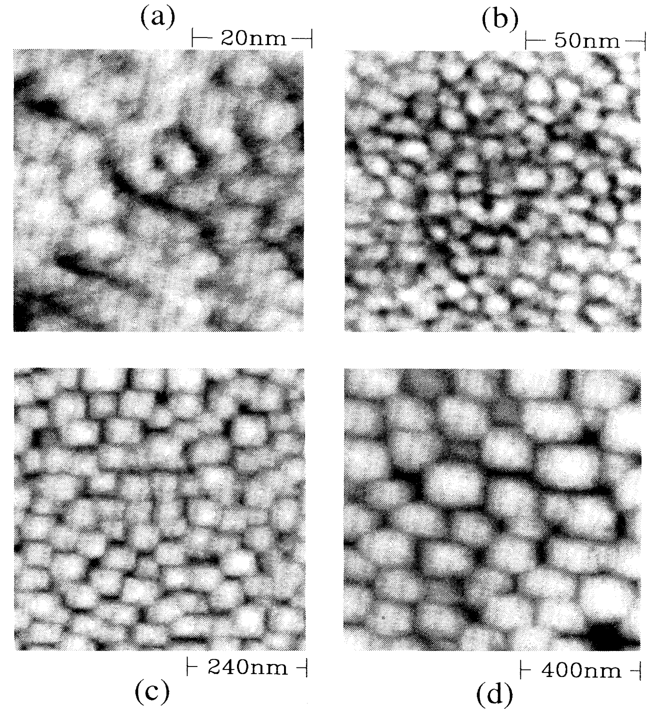


FIG. 2. STM images of growth mounds on Ge(001) grown by MBE over a wide range of temperatures. Scale bars are shown below each image. Thickness of the epitaxial layer, growth temperature, and the black-to-white grey scales are: (a) 5 nm, 60 °C, 1.6 nm; (b) 10 nm, 100 °C, 2.6 nm; (c) 100 nm, 155 °C, 3.1 nm; and (d) 1 $\mu$m, 230 °C, 6.3 nm.

To provide a quantitative analysis of the surface roughness of our epitaxial layers, we calculate the mean correlated height difference [26], $G(\rho) = \langle (h_j - h_i)^2 \rangle$, where $h_j$ and $h_i$ are the heights of the surface at two locations labeled by $i$ and $j$ separated by a distance $\rho$. The brackets signify an average over pairs of points $i, j$ separated by $\rho$. The dynamic scaling hypothesis states that for small $\rho$, $G(\rho) \propto \rho^{2\alpha}$ independent of film thickness and that for large $\rho$, $G(\rho) \propto t^{2\beta}$ where $t$ is the film thickness [26].

In Fig. 3(a), we plot $[G(\rho)]^{1/2}$ for the surface morphologies shown in Figs. 2(a) and 2(d) (our lowest and highest growth temperatures). The dynamic scaling hypothesis does not predict the existence of the growth mounds that dominate the images shown in Fig. 2, but for small $\rho$, $G(\rho)$ for both films, in agreement with dynamic scaling, follows an approximate power-law behavior with $\alpha = 0.8 \pm 0.05$ over a limited range of length scales. Interestingly, the power-law behavior of $G(\rho)$ for the 60 °C growth temperature extends to $\rho = 0.1$ nm, a distance far smaller than the spacing between adjacent dimers on the Ge(001) surface, 0.4 nm. The growth mounds produce only a weak local minimum in $G(\rho)$; the average sepa-

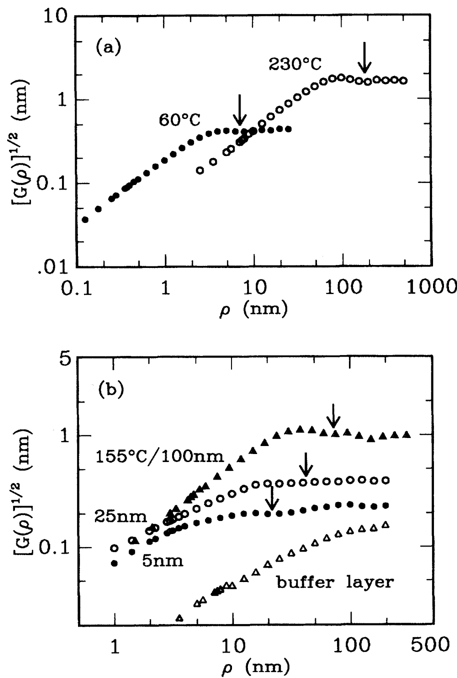


FIG. 3. Root mean correlated height difference $[G(\rho)]^{1/2}$ of surface points separated by a distance $\rho$ for Ge(001) grown by MBE as measured by STM. Arrows mark the average separation between growth features. (a) 5 nm thick film grown at 60° and 1 $\mu$m thick film grown at 230 °C. For topography images, see Figs. 2(a) and 2(d). (b) Films grown at 155 °C. Thickness of each film is labeled in nm. Data for a buffer layer deposited at 365 °C are included for comparison. Topography of the 100 nm thick film is shown as Fig. 2(c).

ration between growth mounds is more easily determined from the corresponding maximum in the height correlation function $\langle h_i h_j \rangle$ (calculation not shown) and is marked by arrows in Fig. 3(a).

While the emphasis of our work is an exploration of the growth morphology at widely different temperatures, we have also examined the evolution of the morphology for different thicknesses deposited at the same temperature. $[G(\rho)]^{1/2}$ for three films deposited at 155 °C is shown in Fig. 3(b). [The topography of only one of these films, 100 nm thick, is shown in Fig. 2(c)]. A highly regular pattern of growth mounds in not observed for 25 nm and 5 nm thick films grown at this temperature, but an average separation $d$ between growth features can again be determined from a weak minimum in $G(\rho)$ or the corresponding maximum in the height correlation function. We observe that $d$ increases with film thickness $t$ in a manner that is consistent with a power law, $d \propto t^{\gamma}$; $\gamma \simeq 0.4$. We have not yet determined if this coarsening behavior is independent of growth temperature.

Figures 3(a) and 3(b) also show that the magnitude of the surface roughness is always small compared to the film thickness. Even at our lowest growth temperature, 60 °C, the surface roughness of a 5 nm thick film is less than 0.5 nm. This relatively small value for the surface roughness, in agreement with XTEM of MBE grown Si(001) [27] and atomic force microscopy of MBE grown GaAs(001) [19] and InP(001) [10], contrasts sharply with the evolution of surface morphology during low temperature MBE growth of Pt(111) [28] and Cu(001) [11]. For these metal surfaces, the motion of adatoms across descending steps is apparently so strongly suppressed that the surface roughens dramatically after only a few monolayers of deposition [29].

A simple model shows that the height of the growth mounds cannot be explained by statistical fluctuations in the growth flux in combination with smoothing of the surface by diffusion [4]. For a film of thickness $t$ monolayers, the statistical fluctuations in the number of atoms deposited into an area $A$ are $(At)^{1/2}$. After smoothing of the area $A$ by surface diffusion, the average height of an area $A$ has fluctuations $\sim(t/A)^{1/2}$ monolayers. Assuming that the mounds cover one-half of the surface area, this model predicts an rms surface roughness for our 60 °C film that is a factor of 5 smaller than what we observe. The discrepancy between this model and our experiments increases to a factor of 30 for a 1 $\mu$m thick film grown at 230 °C.

The failure of this statistical model to account for the magnitude of the surface roughness and the striking similarity of our results to the computational and theoretical results of Ref. [14] lead us to believe that diffusion bias plays an important role in producing the observed surface morphologies. A detailed comparison of our results to theoretical predictions [14] would require a microscopic understanding of the origins of the diffusion bias on Ge(001). Unfortunately, theory and experiment reach opposite conclusions concerning the existence of an asymmetry in the incorporation of adatoms at ascending and descending steps on the related Si(001) surface. Experiments [30] using submonolayer deposition of Si on a Si(001) surface with $\langle 100 \rangle$ oriented steps show that the kinetics of adatom attachment at ascending and descending steps is symmetric. On the other hand, computer simulation [31] of the motion of Si adatoms on Si(001) demonstrate that an adatom approaching a descending type-B step has a significant probability of being reflected. Energy calculations [32] also suggest that an additional energy barrier exists for adatom motion across a descending type-B step. A direct comparison of growth experiments and the theoretical work of Ref. [14] is further complicated by the small size of the step-edge energy barriers needed to produce growth mounds in the Monte Carlo simulation [14].

Experiments on GaAs(001) and simulation [14] suggest that the slope of the sides of the growth mounds is approximately independent of film thickness. To test this hypothesis on Ge(001), we calculate the local slope $\theta$ of the surface in a $10 \times 10$ nm$^2$ area surrounding each pixel of the topography data and compile a histogram that describes the distribution of local slopes $P(\theta)$. For example, if the growth mounds were perfectly pyramidal, $P(\theta)$ would be sharply peaked at the angle of inclination

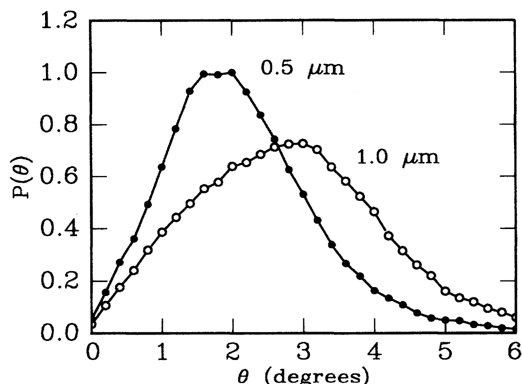


FIG. 4. Distribution $P(\theta)$ of local slopes $\theta$ for a 0.5 $\mu$m and a 1.0 $\mu$m thick film grown at 230 °C. $P(\theta)$ of both films have been scaled by the same factor to set the maximum of $P(\theta)$ for the 0.5 $\mu$m film equal to unity. Topography of the 1.0 $\mu$m thick film is shown in Fig. 2(d).

of the sides of the pyramids. $P(\theta)$ for two thicknesses of films grown at 230 °C are shown in Fig. 4. For this growth temperature, small area STM scans reveal narrow terraces separated by atomic height steps. Growth mounds dominate the large area surface morphology of both films [the topography of only the 1 $\mu$m thick film is shown in Fig. 2(d)], and the average separation between growth mounds increases modestly, 170 to 190 nm, with a doubling in film thickness from 0.5 to 1.0 $\mu$m. The peak in $P(\theta)$, however, shifts from less than 2 to nearly 3 degrees. If we identify the peak in $P(\theta)$ as corresponding to the slope of the sides of the growth mounds, we see that this slope increases significantly with film thickness.

Finally, we comment on the relevance of these results for understanding the critical thickness $h_{\mathrm{epi}}$ for epitaxial growth. Si(001) [24,27] and Ge(001) [25] are known to grow epitaxially at low temperatures up to a limiting thickness $h_{\mathrm{epi}}$ that is a strong function of growth temperature; growth beyond $h_{\mathrm{epi}}$ results in amorphous material. A buildup of surface roughness precedes the crystalline to amorphous transition. The surface roughness is thought to expose {111} facets [25] that produce a breakdown in epitaxial growth. These facts suggest that a predictive model of the dependence of $h_{\mathrm{epi}}$ on growth temperature and deposition rate will require full knowledge of the evolution of surface morphology during multilayer growth. Our observation that a regular pattern of growth mounds is a characteristic feature of multilayer growth over a wide range of temperatures provides a first step toward a quantitative understanding of the connections between surface morphology and $h_{\mathrm{epi}}$.

This work was supported by the U.S. Department of Energy Grant No. DEFG02-91-ER45439 through the University of Illinois Materials Research Laboratory, the Donors of the Petroleum Research Fund, ONR, JSEP, and SRC. We thank Doug Jeffers and Ken Patterson for their assistance with the MBE equipment and Angus Rockett and Brad Orr for helpful discussions.

[1] H.-J. Grossman and E. F. Schubert, Crit. Rev. Solid State Mater. Sci. **18**, 1 (1993).
[2] J. Tersoff, A. W. Denier van der Gon, and R. M. Tromp, Phys. Rev. Lett. **72**, 266 (1994).
[3] D. D. Vvedensky, A. Zangwill, C. N. Luse, and M. R. Wilby, Phys. Rev. A **48**, 852 (1993).
[4] J. Villain, J. Phys. I (France) **1**, 19 (1991).
[5] J. Chevrier, V. Le Thanh, R. Buys, and J. Derrien, Europhys. Lett. **16**, 737 (1991).
[6] R. Chiarello, V. Panella, J. Krim, and C. Thompson, Phys. Rev. Lett. **67**, 3408 (1991).
[7] R. C. Salvarezza, L. Vazquez, P. Herrasti, P. Ocon, J. M. Vara, and A. J. Arvia, Europhys. Lett. **20**, 727 (1992).
[8] Y.-L. He, H.-N. Yang, T.-M. Lu, and G.-C. Wang, Phys. Rev. Lett. **69**, 3770 (1992).
[9] H. You, R. P. Chiarello, H. K. Kim, and K. G. Vandervoort, Phys. Rev. Lett. **70**, 2900 (1993).
[10] M. A. Cotta *et al.,* Phys. Rev. Lett. **70**, 4106 (1993).
[11] H.-J. Ernst, F. Fabre, R. Folkerts, and J. Lapujoulade, Phys. Rev. Lett. **72**, 112 (1994).
[12] C. Thompson, G. Palasantzas, Y. P. Feng, S. K. Sinha, and J. Krim, Phys. Rev. B **49**, 4902 (1994).
[13] William M. Tong *et al.,* Phys. Rev. Lett. **72**, 3374 (1994).
[14] M. D. Johnson, C. Orme, A. W. Hunt, D. Graff, J. Sudijono, L. M. Sander, and B. G. Orr, Phys. Rev. Lett. **72**, 116 (1994).
[15] Gert Ehrlich and F. G. Hudda, J. Chem. Phys. **44**, 1039 (1966).
[16] S. C. Wang and Gert Ehrlich, Phys. Rev. Lett. **67**, 2509 (1991).
[17] G. S. Bales and A. Zangwill, Phys. Rev. B **41**, 5500 (1990).
[18] G. W. Smith *et al.,* J. Cryst. Growth **127**, 966 (1993).
[19] C. Orme, M. D. Johnson, J. L. Sudijono, K. T. Leung, and B. G. Orr, Appl. Phys. Lett. **64**, 860 (1994).
[20] M. A. Cotta, R. A. Hamm, S. N. G. Chu, L. R. Harriot, and H. Temkin, J. Appl. Phys. **75**, 630 (1994).
[21] X.-J. Zhang *et al.,* J. Vac. Sci. Technol. A **11**, 2553 (1993).
[22] M. Copel and R. M. Tromp, Phys. Rev. Lett. **72**, 1236 (1994).
[23] H. Jorke, H.-J. Herzog, and H. Kibbel, Phys. Rev. B **40**, 2005 (1989).
[24] D. J. Eaglesham, H.-J. Grossmann, and M. Cerullo, Phys. Rev. Lett. **65**, 1227 (1990).
[25] G. Xue, H. Z. Xiao, M.-A. Hasan, J. E. Greene, and H. K. Birnbaum, J. Appl. Phys. **74**, 2512 (1994).
[26] Jean Lapujoulade, Surf. Sci. Rep. **20**, 191 (1994).
[27] D. P. Adams, S. M. Yalisove, and D. J. Eaglesham, Appl. Phys. Lett. **63**, 3571 (1993).
[28] B. Poelsema, R. Kunkel, N. Nagel, A. F. Becker, G. Rosenfeld, L. K. Verheij, and G. Comsa, Appl. Phys. A **53**, 369 (1991).
[29] Michael Bott, Thomas Michely, and George Comsa, Surf. Sci. **272**, 161 (1994).
[30] Y.-W. Mo and M. G. Lagally, Surf. Sci. **248**, 313 (1991).
[31] Deepak Srivastava and Barbara J. Garrison, Phys. Rev. B **47**, 4464 (1993).
[32] Zhenyu Zheng, Yan-Ten Lu, and Horia Metiu, Phys. Rev. B **46**, 1917 (1992).

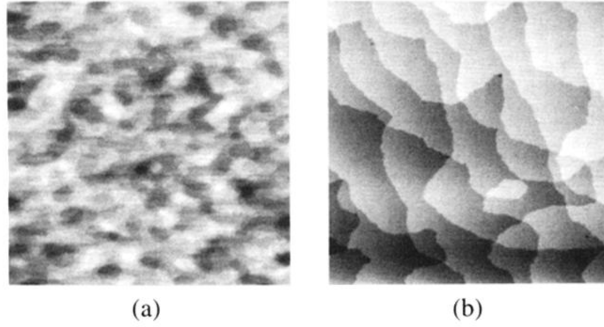


FIG. 1. STM images of Ge(001) following (a) oxide desorption and annealing at 450 °C and (b) growth of a 100 nm thick buffer layer at 365 °C. The $x$-$y$ range of both images is 1 $\mu$m and the $x$ and $y$ axes of the images are aligned with the $\langle 100 \rangle$ crystal directions.

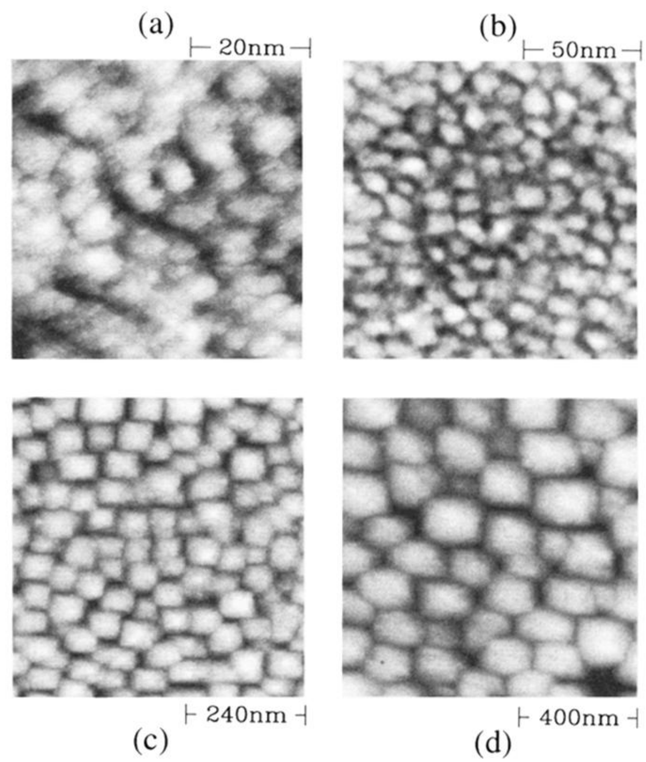


FIG. 2. STM images of growth mounds on Ge(001) grown by MBE over a wide range of temperatures. Scale bars are shown below each image. Thickness of the epitaxial layer, growth temperature, and the black-to-white grey scales are: (a) 5 nm, 60 °C, 1.6 nm; (b) 10 nm, 100 °C, 2.6 nm; (c) 100 nm, 155 °C, 3.1 nm; and (d) 1 $\mu$m, 230 °C, 6.3 nm.